Chaos, Solitons and Fractals 189 (2024) 115614

Contents lists available at ScienceDirect

Chaos, Solitons and Fractals

journal homepage: www.elsevier.com/locate/chaos

Ratchet current and scaling properties in a nontwist mapping

Matheus Rolim Sales [a,*], Daniel Borin [a], Leonardo Costa de Souza [b], José Danilo Szezech Jr. [c,d], Ricardo Luiz Viana [e], Iberê Luiz Caldas [b], Edson Denis Leonel [a]

[a] Departamento de Física, Universidade Estadual Paulista (UNESP), 13506-900, Rio Claro, SP, Brazil
[b] Instituto de Física, Universidade de São Paulo, 05315-970, São Paulo, SP, Brazil
[c] Programa de Pós-Graduação em Ciências, Universidade Estadual de Ponta Grossa, 84030-900, Ponta Grossa, PR, Brazil
[d] Departamento de Matemática e Estatística, Universidade Estadual de Ponta Grossa, 84030-900, Ponta Grossa, PR, Brazil
[e] Departamento de Física, Universidade Federal do Paraná, 81531-990, Curitiba, PR, Brazil

ARTICLE INFO

Keywords:
Ratchet effect
Unbalanced stickiness
Scaling invariance
Critical exponents

ABSTRACT

We investigate the transport of particles in the chaotic component of phase space for a two-dimensional, area-preserving nontwist map. The survival probability for particles within the chaotic sea is described by an exponential decay for regions in phase space predominantly chaotic and it is scaling invariant in this case. Alternatively, when considering mixed chaotic and regular regions, there is a deviation from the exponential decay, characterized by a power law tail for long times, a signature of the stickiness effect. Furthermore, due to the asymmetry of the chaotic component of phase space with respect to the line $I = 0$, there is an unbalanced stickiness that generates a ratchet current in phase space. Finally, we perform a phenomenological description of the diffusion of chaotic particles by identifying three scaling hypotheses, and obtaining the critical exponents via extensive numerical simulations.

1. Introduction

The phase space of a two-dimensional integrable Hamiltonian system is composed of periodic and quasiperiodic invariant tori. When a weak perturbation is introduced into such a system, according to the Kolmogorov-Arnold-Moser (KAM) theorem [1], the sufficiently irrational tori survive the perturbation (KAM tori), while the rational ones are destroyed. Near the original position of the destroyed rational tori, emerges a set of elliptical and hyperbolic fixed points, as outlined by the Poincaré-Birkhoff theorem [1]. The chaotic motion appears in the vicinity of the hyperbolic fixed points due to their unstable nature, while the elliptical points are the centers of the regular regions, hereafter named stability islands. The coexistence of chaotic and regular regions in two-dimensional quasi-integrable Hamiltonian system makes its phase space neither integrable nor uniformly hyperbolic. The phase space is divided into distinct and unconnected domains, where the chaotic orbits fill densely the available region in phase space and the stability islands consist of periodic and quasiperiodic orbits that lie on invariant tori. Furthermore, an orbit initially in the chaotic sea will never enter any island, and the periodic and quasi-periodic orbits will never reach the chaotic sea [1,2].

For increasing perturbation strength, the KAM tori are also destroyed and their remnants form a Cantor set known as cantori [2–4]. The role of the KAM tori and the cantori in the transport of particles in phase space differs fundamentally. While the KAM tori are full barriers to the transport in phase space, the cantori act as partial barriers, allowing particles to pass through them. When a particle crosses a cantorus, it might stay trapped in the region bounded by the cantorus for a long, but finite, period of time, during which it behaves similarly as a quasiperiodic orbit, until it escapes to the chaotic sea. This intermittence in the dynamics of a chaotic orbit is the phenomenon of stickiness [4–12]. The structure of stability islands embedded in the chaotic sea and cantori organize itself in a hierarchical structure of islands-around-islands, where the larger islands are surrounded by smaller islands, which are in turn surrounded by even smaller islands and so on for increasingly smaller scales [13,14]. In this way, during the time a chaotic orbit is trapped in a region bounded by a cantorus, it might cross inner cantori for arbitrarily small scales and thus stay trapped for longer times. This long times affects the statistical properties of the transport of particles in phase space [15–18], as well as the recurrence time statistics [19–24], the survival probability [10,25–35], and the decay of correlations [6–8,36,37].

About two decades ago, a new feature was observed in the transport of particles in the chaotic component of phase space in Hamiltonian systems: the existence of a preferential direction for the transport without an external bias, the so-called Hamiltonian ratchet [38–44]. The ratchet

* Corresponding author.
E-mail address: rolim.sales@unesp.br (M. Rolim Sales).

https://doi.org/10.1016/j.chaos.2024.115614
Received 17 June 2024; Received in revised form 11 September 2024; Accepted 1 October 2024
Available online 10 October 2024

effect is defined by a directed current, or ratchet current, which is a preferential direction for the transport of particles in phase space without an external bias. This phenomenon has applications on a variety for physical systems such as Josephson junctions [45,46], Brownian [47] and molecular [48] motors, cold atom systems [49–52], and electronic transport in superlattices [53,54], to cite a few. Initial studies focused on the role of the external noise [47,55,56], which was later replaced by a deterministic chaotic dynamics with inertia terms in the equations of motion [57–60]. Nonetheless, even purely Hamiltonian dynamics with mixed [38–41,43,44] or completely chaotic [42] phase space can generate a ratchet current. It was demonstrated that the ratchet effect is a consequence of spatial and/or temporal symmetry breaking of the system [39,41,44,61]. Furthermore, Mugnaine et al. [62] demonstrated that due to a symmetry breaking in the extended standard nontwist mapping [63,64], the twin island scenario no longer exists, implying a ratchet current in phase space due to the emergence of an unbalanced stickiness in different regions in phase space.

The anomalous transport of particles in magnetized plasmas is heavily impacted by the $\mathbf{E}\times\mathbf{B}$ drift motion, caused by fluctuations in the plasma [65]. In the case of passive particle transport, where the particles do not alter the electric field, the problem is described by a Hamiltonian system [66]. Furthermore, given the divergence-free nature of magnetic fields, the field lines can be described by a two-dimensional area-preserving mapping, with respect to the surface of section of the torus at a fixed toroidal angle [67]. In this paper, we study transport properties and diffusion for a nontwist mapping, introduced in the context of $\mathbf{E}\times\mathbf{B}$ drift in toroidal plasmas [68–70], in the transition from integrability (zero perturbation) to non-integrability (small perturbation) when the phase space is bounded. In the context of magnetic confined plasmas, as in Tokamak devices [71,72], the use of non-monotonic profiles for physical quantities is related to nontwist effects like the existence of a shearless curve that acts as a robust barrier preventing the chaotic orbits from escaping the plasma [73]. Nontwist Hamiltonian systems are characterized by complex dynamics, including the formation of transport barriers and intricate island structures. Understanding these chaotic transport processes is essential for predicting and controlling plasma behavior.

Initially, we analyze the survival probability by introducing two exits symmetrically apart from the line $I = 0$ and show that as long as there are no stability islands within the survival regions, the survival probability follows an exponential decay, and the decay rate scales as a power law with the limits of the survival regions. Furthermore, the survival probability exhibits scaling invariance with respect to the limits of the survival regions. Then, we consider two different ensembles of initial conditions, both with $\langle I\rangle \approx 0$ initially. The first ensemble is uniformly distributed along the whole survival region and we calculate the escape times and the escape basins for different survival region limits. We find that the measure of the bottom basin increases with the survival region area due to the inclusion of stability islands within this region. This ensemble, however, might be biased due to the distribution of initial conditions in phase space. To avoid this potential bias, we consider a second ensemble randomly distributed in a small region around the line $I = 0$ and calculate the fraction of particles that escape from the top and bottom exits. We find, once again, that as we change the size of the survival region and islands start to appear, there is a tendency for the particles to escape through the bottom exit. Also, we observe a nonzero space average of the action, $\langle I\rangle$, characteristic of the ratchet effect.

As for the mechanism behind such a phenomenon, we calculate the distribution of recurrence times considering the upper ($I > 0$) and lower ($I < 0$) regions of phase as our recurrence regions. We find that the cumulative distribution of recurrence times for these regions are different for long times, indicating that the chaotic orbits sticky unevenly in the upper and lower regions, *i.e.*, there is an unbalanced stickiness in phase space. The first and higher moments of the distribution of recurrence times are also different, consolidating that the two distributions are, in fact, different. Lastly, we investigate the scaling properties of diffusion in phase space. We choose as our observable the square root of the averaged squared action, I_{rms}, and we obtain the critical exponents that describe the behavior of I_{rms}. These quantities are described in terms of three scaling hypotheses, leading to a robust analysis of the scaling invariance observed for our observable.

This paper is organized as follows. In Section 2 we describe the mapping under study and present some of its properties. In Section 3 we study the transport properties of the chaotic component of phase space. We begin by calculating the survival probability for different survival regions and in the sequence, we investigate whether the system exhibits unbiased transport by considering two different ensembles of initial conditions with zero initial average action. In Section 4 we present a phenomenological description of diffusion in the chaotic component of phase space. We obtain the critical exponents and compare our results with similar results in the literature. Section 5 contains our final remarks.

2. The model and its properties

The Hamiltonian function of an autonomous two degrees of freedom system is often written as [1]

$$H(I_1, I_2, \theta_1, \theta_2) = H_0(I_1, I_2) + \varepsilon H_1(I_1, I_2, \theta_1, \theta_2), \tag{1}$$

where (I_i, θ_i) are the canonical action–angle variables, H_0 is the integrable term and εH_1 is a perturbation to the integrable system, with ε controlling the transition from integrability ($\varepsilon = 0$) to non-integrability ($\varepsilon > 0$). The solution of Eq. (1) is a four-dimensional flow. However, since $\partial H/\partial t = 0$, the Hamiltonian equals the total mechanical energy of the system, $H = E = T + V$, and it is a constant of motion. This allows us to eliminate one of the variables, *e.g.* I_2, from H, making it possible to write $H = H(I_1, \theta_1, \theta_2, E)$. Therefore, orbits with energy E are restricted to lie on a three-dimensional energy surface on the four-dimensional phase space. It is possible to decrease the dimension even further by considering an appropriate Poincaré section. We choose the plane $\theta_1 \times I_1$ with θ_2 constant as our Poincaré section, resulting in a two-dimensional mapping described by the following equations:

$$\begin{aligned} I_{n+1} &= I_n + \varepsilon h(\theta_n, I_{n+1}), \\ \theta_{n+1} &= \theta_n + K(I_{n+1}) + \varepsilon p(\theta_n, I_{n+1}) \mod 2\pi, \end{aligned} \tag{2}$$

where $h(\theta_n, I_{n+1})$, $K(I_{n+1})$, and $p(\theta_n, I_{n+1})$ are nonlinear functions of their arguments and this mapping relates the $(n+1)$th intersection and the previous nth intersection with the Poincaré section. The mapping in Eq. (2) is area-preserving if the nonlinear functions satisfy the following condition

$$\frac{\partial p(\theta_n, I_{n+1})}{\partial \theta_n} + \frac{\partial h(\theta_n, I_{n+1})}{\partial I_{n+1}} = 0. \tag{3}$$

Considering $p(\theta_n, I_{n+1}) \equiv 0$ and $h(\theta_n, I_{n+1}) = \sin(\theta_n)$, and changing $K(I_{n+1})$ we obtain different systems well known in the literature, such as

- $K(I_{n+1}) = I_{n+1}$: the standard mapping [74].
- $K(I_{n+1}) = 2/I_{n+1}$: the static wall approximation of the Fermi–Ulam model [75,76].
- $K(I_{n+1}) = \delta I_{n+1}$: the simplified bouncer model [77,78].
- $K(I_{n+1}) = I_{n+1} + \delta I_{n+1}^2$: the logistic twist map [79].
- $K(I_{n+1}) = |I_{n+1}|^{-\gamma}$: the Leonel mapping [35,80–84].

In this paper, we consider the drift motion $\mathbf{E}\times\mathbf{B}$ in a toroidal plasma, where the electric field is generated by the combination of an external radial field E and electrostatic potential $\tilde{\phi}$ generated by fluctuations in the plasma. The equations of the drift motion $\mathbf{E}\times\mathbf{B}$ are

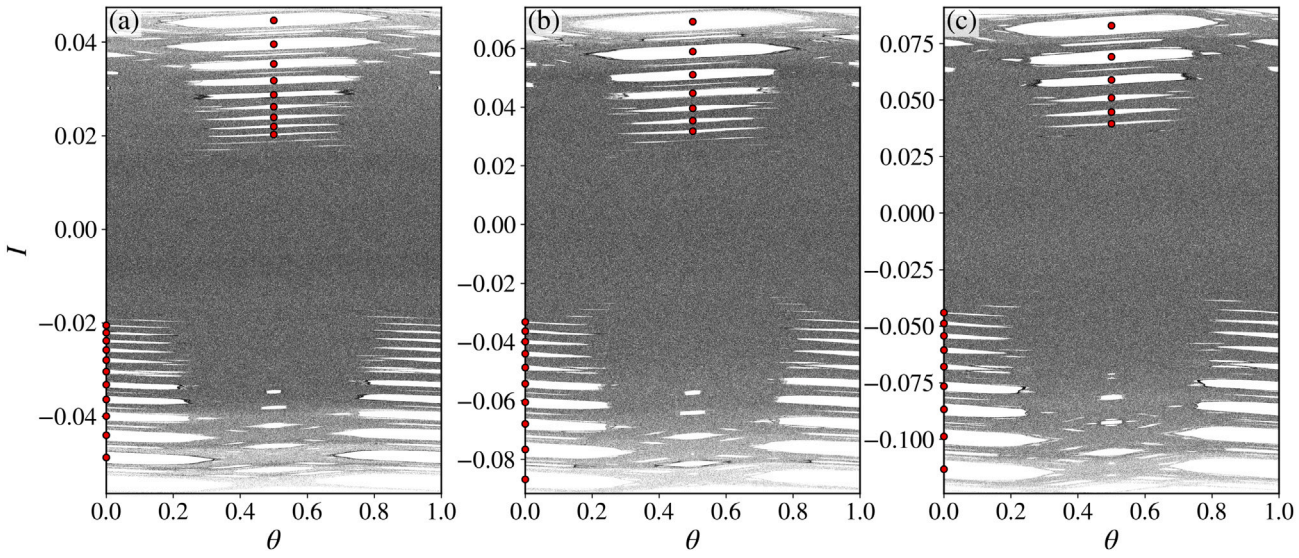

Fig. 1. The phase space of the mapping Eq. (4) for 375 randomly chosen initial conditions within the chaotic sea with (a) $\varepsilon = 1.0\times10^{-3}$, (b) $\varepsilon = 2.0\times10^{-3}$, and (c) $\varepsilon = 3.0\times10^{-3}$. The red dots correspond to elliptic points at the center of the period-1 islands.

Table 1
Parameter values of the two-dimensional area-preserving nontwist Hamiltonian mapping, Eq. (4).

q_1	5.0	e_3	4.13	M	15
q_2	−6.3	v_1	−9.867	L	6
q_3	6.3	v_2	17.47	μ	1.83×10^{-2}
e_1	10.7	v_3	10.1	ρ	-9.16×10^{-1}
e_2	−15.8	v_4	−9.0	–	–

given by the following nontwist, area-preserving mapping [68–70]

$$\begin{aligned} I_{n+1} &= I_n + \varepsilon\sin(2\pi\theta_n),\\ \theta_{n+1} &= \theta_n + \mu v(I_{n+1})\left[\frac{M}{q(I_{n+1})} - L\right]\\ &\quad + \rho\frac{E(I_{n+1})}{\sqrt{|I_{n+1}|}} \mod 1, \end{aligned} \tag{4}$$

where $q(I)$, $E(I)$, and $v(I)$ are nonmonotonic functions, representing the safety factor, external applied radial electric field, and toroidal plasma velocity, respectively. The non-monotonicity of these functions makes the system violate the twist condition, which implies different dynamical properties [79,85]. The nonmonotonic functions are given by,

$$\begin{aligned} q(I) &= q_1 + q_2 I^2 + q_3 I^3,\\ E(I) &= e_1 I + e_2\sqrt{|I|} + e_3,\\ v(I) &= v_1 + v_2\tanh(v_3 I + v_4), \end{aligned}$$

Although this mapping has many parameters, our only control parameter is ε and the remaining parameters are chosen accordingly to Refs. [69,70] and can be found in Table 1. The parameter ε is proportional to the amplitude of the electrostatic instabilities that generate the drift motion. Thus, it is the control parameter of integrability of the system. For the integrable case without perturbation ($\varepsilon = 0$), the variable I is positive. However, with the perturbation I can reach small negative values.

Similarly to the Leonel mapping [35,80–84], when the action I_n is small, the angles θ_n and θ_{n+1} become uncorrelated due to the divergence of the second equation in Eq. (4), thus producing chaotic regions for nonzero perturbation. For larger values of the action, the angles become correlated and regularity appears as stability islands and invariant spanning curves. In Fig. 1 we show the phase space of the mapping (4) for different perturbation values. For $\varepsilon = 0$ (not shown) the mapping reduces to a nontwist radial map due to the nonmonotonicity of the functions $q(I)$, $E(I)$, and $v(I)$. In this case, the mapping is regular, the system is integrable, I_n is constant, and the phase space has only periodic and quasiperiodic structures. On the other hand, for $\varepsilon > 0$ the regularity is broken, even for $\varepsilon \ll 1$, and the phase space becomes mixed. There is a coexistence of chaotic and regular domains and as ε increases, the chaotic region expands in the vertical direction due to the breaking of the KAM curves. For the chosen parameter values, the phase space is bounded, *i.e.*, the transport in the vertical direction is confined to a finite area. Interestingly, the limits of the chaotic component shown in Fig. 1 are not symmetric with respect to the $I = 0$ line.

The majority of stability islands for the considered values of ε correspond to period-1 islands, which are centered around fixed elliptic points. The fixed points can be found from the following conditions:

$$\begin{aligned} I_{n+1} &= I_n = I^*,\\ \theta_{n+1} &= \theta_n = \theta^* + m, \end{aligned} \tag{5}$$

where m is an integer. Substituting Eqs. (5) into Eqs. (4), the fixed points must satisfy

$$\begin{aligned} \sin(2\pi\theta^*) &= 0,\\ \mu v(I^*)\left[\frac{M}{q(I^*)} - L\right] + \rho\frac{E(I^*)}{\sqrt{|I^*|}} &= m. \end{aligned} \tag{6}$$

The first equation can be easily solved to find $\theta^* = 0, 0.5$. The second equation, however, cannot be solved analytically. We solve it numerically using the *fsolve* function from the *Scipy* module [86], which uses Powell's hybrid method, and the red dots in Fig. 1 correspond to the elliptical fixed points found for different integers m.

We characterize the chaotic component of the phase space using the Lyapunov exponents [87–90]. Given a mapping $\mathbf{f} : \mathbb{R}^d \to \mathbb{R}^d$, defined as $\mathbf{x}_{n+1} = \mathbf{f}(\mathbf{x}_n) = \mathbf{f}^n(\mathbf{x}_0)$, let $\mathbf{Df}^n$ be the n iterate of the Jacobian matrix. We define the infinite-time Lyapunov exponents as

$$\lambda_i^{\infty} = \lim_{n\to\infty}\frac{1}{n}\ln\left(\|\mathbf{Df}^n u_i\|\right), \tag{7}$$

where u_i is the eigenvector corresponding to the ith eigenvalue of $\mathbf{Df}^n$. A d-dimensional system has d characteristic Lyapunov exponents, and we say the system is chaotic if at least one of them is positive. Furthermore, for Hamiltonian systems, which preserve volume in phase space under time evolution (Liouville's theorem) [1], the sum of all Lyapunov exponents must equal zero. Hence, for our two-dimensional area-preserving mapping, there are two characteristic exponents and

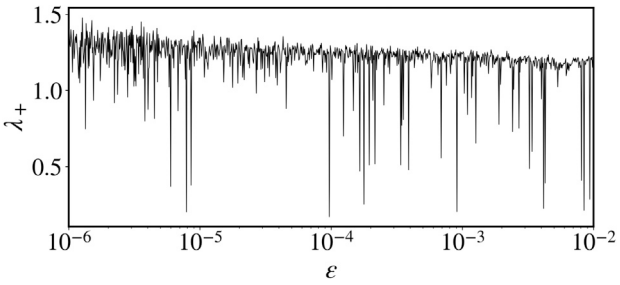

Fig. 2. Largest Lyapunov exponent as a function of ε with initial condition $(\theta_0, I_0) = (0.5, 1.0\times10^{-10})$ and total iteration time $N = 1.0\times10^8$.

they satisfy $\lambda_+ \equiv \lambda_1 = -\lambda_2$. In this case, all regular orbits, *i.e.*, periodic, or quasi-periodic have zero Lyapunov exponents for infinite times, while chaotic orbits exhibit $\lambda_+ > 0$. In Fig. 2 we show the largest Lyapunov exponent, λ_+, as a function of the control parameter ε for a single initial condition. We change ε in a large interval and notice that λ_+, on the other hand, does not change significantly when compared to the range of variation of ε. This nearly constant value of λ_+ indicates that the chaotic component in phase space is scaling invariant with respect to the control parameter ε [84]. We study such scaling properties in Sections 3 and 4.

3. Survival probability and ratchet current

In this section, we explore the transport of particles in the chaotic component of phase space. We have seen in the previous Section that the phase space for $\varepsilon \ll 1$ is bounded, and therefore the particle is confined within a finite area. We consider two exits placed symmetrically from the $I = 0$ line, and they define the survival region, $(\theta, I) \in [0, 1)\times[-I_{\rm esc}, I_{\rm esc}]$ (Fig. 3). We consider an ensemble of $M = 10^6$ particles randomly distributed in $(\theta, I) \in [0, 1)\times[-1.0\times10^{-10}, 1.0\times10^{-10}]$. We evolve each particle to at most $N = 10^6$ times, and if the particle reaches one of the exits, *i.e.*, if $I_n = \pm I_{\rm esc}$, it escapes and we interrupt the evolution of this particle and initialize another particle. We repeat this procedure until the whole ensemble is exhausted. From this ensemble, we calculate the survival probability, $P(n)$, that corresponds to the probability of a particle surviving along the dynamics in a given chaotic domain without escaping. In other words, it corresponds to the fraction of particles that have not yet reached one of the exits until the nth iteration. Mathematically, it is defined as $P(n) = N_{\rm surv}(n)/M$, where $N_{\rm surv}(n)$ is the number of particles that have survived until the nth iteration. The behavior of the survival probability depends strongly on the characteristics of phase space. For fully chaotic systems, the survival probability follows an exponential decay [29,31,32,34] given by

$$P(n) = P_0 \exp(-\kappa n), \tag{8}$$

where κ is the decay rate. However, for systems with mixed phase space, the decay is slower and usually characterized by the emergence of a power law tail for long times [10,26,27,30,35] or by stretched exponential [28,33,34]. As has been discussed previously, the stickiness effect, due to the presence of stability islands embedded in the chaotic sea, affects the statistical properties of the transport of particles in phase space. The chaotic orbits might be trapped near these stability islands, leading to long survival times, and causing the deviation from the exponential decay.

We calculate the survival probability for different survival regions, such as the ones shown in Fig. 3, with $\varepsilon = 1.0\times10^{-3}$ [Fig. 4(a)]. We observe the exponential decay for $I_{\rm esc} < 0.02$. For larger survival regions, the survival probability starts with an exponential decay for small times, until the power law tail emerges for long times. We note that the decay remains exponential until $I_{\rm esc}$ reaches the first period-1 stability

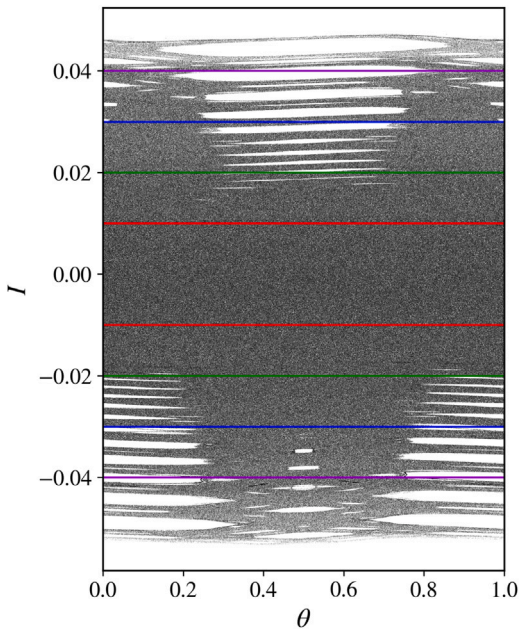

Fig. 3. The phase space of the mapping Eq. (4) for 375 randomly chosen initial conditions within the chaotic sea with $\varepsilon = 1.0\times10^{-3}$. The regions delimited by the colored horizontal lines correspond to the survival regions defined by $(\theta, I) \in [0, 1)\times[-I_{\rm esc}, I_{\rm esc}]$ with (red) $I_{\rm esc} = 0.01$, (green) $I_{\rm esc} = 0.02$, (blue) $I_{\rm esc} = 0.03$, and (violet) $I_{\rm esc} = 0.04$. (For interpretation of the references to color in this figure legend, the reader is referred to the web version of this article.)

island [blue dot on the inset of Fig. 4(b)], where the coordinates for its elliptic fixed point are $(\theta_{fi}, I_{fi}) = (0.5, 0.02026073030486245)$. The smaller islands below the period-1 island shown in the inset do not statistically influence the survival probability. Furthermore, the decay rate, κ, obtained from the optimal fitting based on the function given by Eq. (8), scales with $I_{\rm esc}$ as a power law for $I_{\rm esc} < I_{fi}$ with exponent $\zeta = -1.865 \pm 0.007$ [red dots and red dashed line in Fig. 4(b)]. The knowledge of ζ allows us to rescale the horizontal axis through the transformation $n \to nI_{\rm esc}^{\zeta}$ causing the survival probability curves to overlap onto a single, and hence, universal curve [Fig. 4(c)]. This indicates that the survival probability is scaling invariant for survival regions composed of predominantly chaotic regions ($I_{\rm esc} < I_{fi}$).

Essentially, when some observable of a dynamical system exhibits scaling invariance, its expected behavior remains consistent and robust regardless of scale, *i.e.*, we can rescale the system conveniently such that after a reparametrization, the observable is scale independent and exhibits universal features [91]. The scaling invariance of the survival probability, for instance, has been explored in a variety of systems, such as the Leonel mapping [35], billiard systems [92], and, more recently, on fractional versions of the standard map [93,94].

Let us now investigate how transport occurs for particles uniformly distributed on the survival regions $(\theta, I) \in [0, 1)\times[-I_{\rm esc}, I_{\rm esc}]$ for $I_{\rm esc} = 0.01, 0.02, 0.03, 0.04$. Note that $\langle I\rangle \approx 0$ at $n = 0$ for this ensemble. We consider 1080×1080 initial conditions and iterate each one for at most $N = 10^6$ times. We count the time each particle takes to reach either of the exits (top row of Fig. 5). Black and blue colors indicate a fast escape while the gray color corresponds to particles that have not yet escaped within $N = 10^6$ iterations. The intermediate values of $T_{\rm esc}$ correspond to trapped particles. We observe that in cases of small survival regions, where stability islands are absent or nearly absent, the escape is fast. On the other hand, for the larger survival region considered [Fig. 5(d_1)], most particles remain inside it for long times, with emphasis on the initial conditions near the stability islands (red color).

We also construct the escape basin for these survival regions (bottom row of Fig. 5). Particles that escape through the bottom (top)

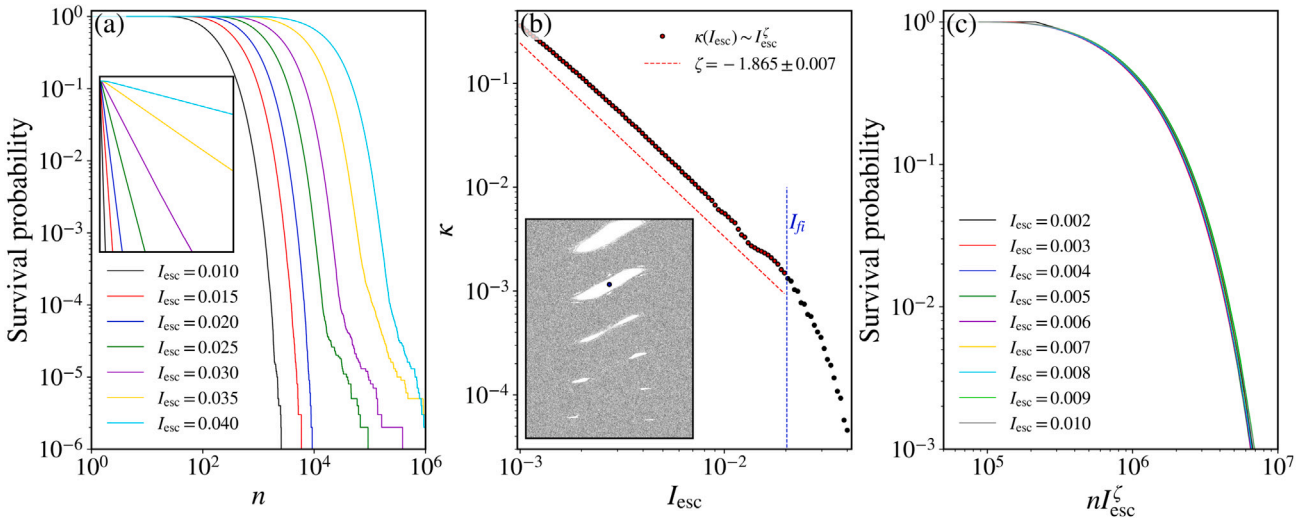

Fig. 4. (a) The survival probability for different survival regions with $\varepsilon = 1.0 \times 10^{-3}$ considering an ensemble of 1.0×10^6 randomly chosen initial conditions on the interval $(\theta, I) \in [0, 1) \times [-1.0 \times 10^{-10}, 1.0 \times 10^{-10}]$. The inset corresponds to a semilog magnification of the region $(n, P) \in [0, 3 \times 10^4] \times [1.0 \times 10^{-3}, 1]$ to observe the exponential decay. (b) The escape rate, κ, is obtained from the optimal fitting considering the function $P(n) \sim e^{-\kappa n}$ for different values of I_{esc}. For I_{esc} small enough, κ obeys a power law (red dots), $\kappa(I_{esc}) \sim I_{esc}^{\zeta}$, with $\zeta = -1.865 \pm 0.007$. (c) The overlap of the survival probability for small I_{esc} onto a single and universal plot after the transformation $n \to nI_{esc}^{\zeta}$. The inset in (b) is a magnification of Fig. 1(a) within the region $(\theta, I) \in [0, 1) \times [0.015, 0.0225]$. The blue dot corresponds to the obtained center of the first period-1 island with coordinates given by $(\theta_{fi}, I_{fi}) = (0.5, 0.02026073030486245)$. For $I_{esc} > I_{fi}$, κ deviates from the power law decay (black dots). (For interpretation of the references to color in this figure legend, the reader is referred to the web version of this article.)

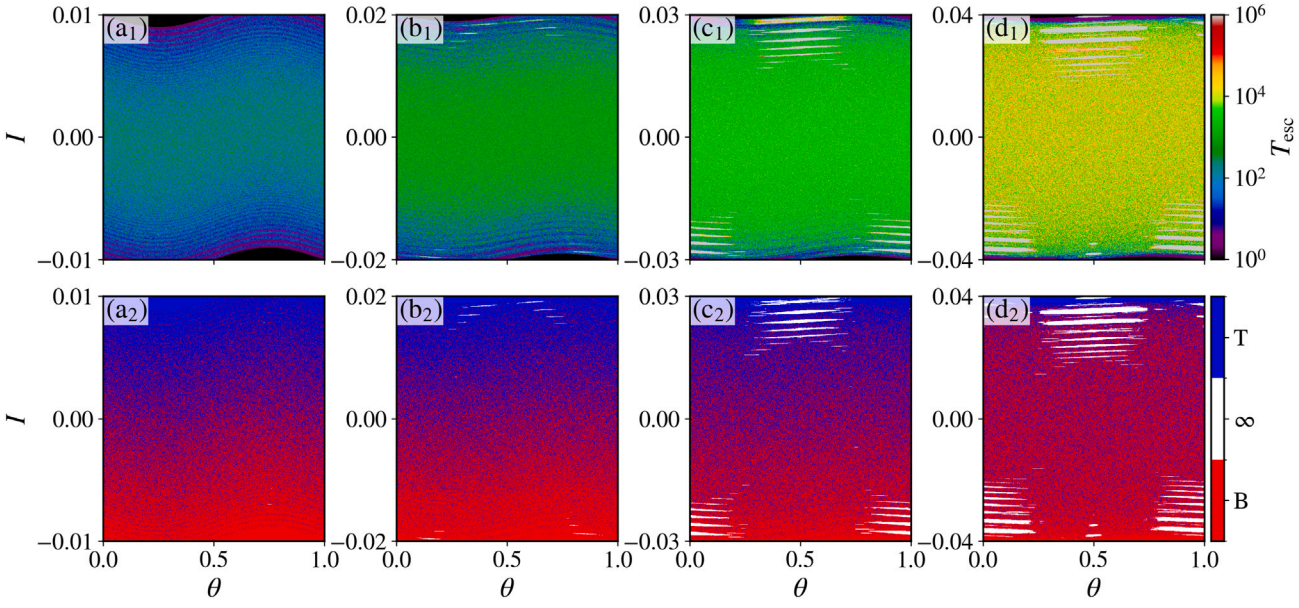

Fig. 5. Escape times (top row) and escape basins (bottom) with $\varepsilon = 1.0 \times 10^{-3}$ for different survival regions, namely, (a) $I_{esc} = 0.01$, (b) $I_{esc} = 0.02$, (c) $I_{esc} = 0.03$, and (d) $I_{esc} = 0.04$. If the particle escapes through the bottom (top) exit, we color the point red (blue). If the particle never escapes the survival region, we color the initial condition white. (For interpretation of the references to color in this figure legend, the reader is referred to the web version of this article.)

exit are colored red (blue), while those that never escape are colored white. Visually, for small survival regions [Fig. 5(a_2) and (b_2)] the red and blue points are distributed in equal measure, without a preferred region. However, for larger survival regions [Fig. 5(c_2) and (d_2)], with the emergence of the stability islands, the red basin appears to have a greater measure than the blue one, indicating a preference for escape through the bottom exit. In Table 2 we show the fraction of initial conditions that escape through the bottom (p_B) and top (p_T) exits, and also the ones that never escape (p_∞), calculated from the escape basins in Fig. 5. Note that $p_B + p_T + p_\infty = 1$. Indeed, the larger the survival region, *i.e.*, the stronger the influence of the stability islands, the larger the ratio p_B/p_T, which corroborates our qualitative analysis of the escape basins: there is a preferential direction for the transport of particles in the chaotic component in phase space.

However, how the particles are distributed in phase space might influence our previous conclusion. For example, some particles could be closer or farther away from the exits, while others might remain trapped for a longer duration. To eliminate this potential bias, we consider an ensemble of 10^6 randomly chosen initial conditions on the interval $(\theta, I) \in [0, 1) \times [-1.0 \times 10^{-10}, 1.0 \times 10^{-10}]$, with $\langle I \rangle \approx 0$. Each particle is iterated up to $N = 10^6$ times. We compute the fraction of particles that escape through either the bottom or top exit as a function of the survival region limits, I_{esc}, for $\varepsilon = 1.0 \times 10^{-3}$, $\varepsilon = 2.0 \times 10^{-3}$, and $\varepsilon = 3.0 \times 10^{-3}$ (Fig. 6). For small survival regions, we observe that

Table 2
Fraction of initial conditions that escape through the bottom (p_B) and top (p_T) exits and that never escapes (p_∞) calculated from the escape basins in Fig. 5.

Fig. 5	p_B	p_T	p_∞	p_B/p_T
(a_2)	0.498364	0.501601	0.000035	0.993548
(b_2)	0.513745	0.484148	0.002107	1.061132
(c_2)	0.502372	0.467406	0.030222	1.074810
(d_2)	0.606776	0.327269	0.065954	1.854058

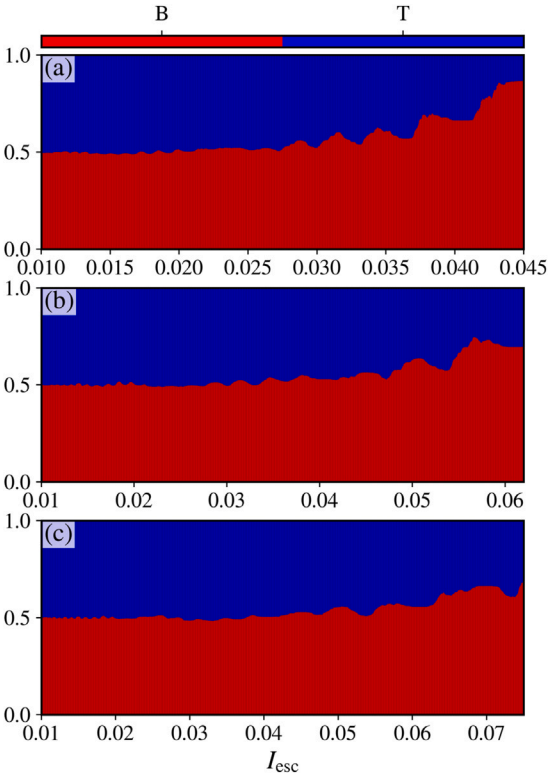

Fig. 6. Fraction of initial conditions that escape through the (red) bottom exit and the (blue) top exit as a function of the exit's position with (a) $\varepsilon = 1.0 \times 10^{-3}$, (b) $\varepsilon = 2.0 \times 10^{-3}$, and (c) $\varepsilon = 3.0 \times 10^{-3}$. We considered an ensemble of 10^6 randomly chosen initial conditions on the interval $(\theta, I) \in [0, 1) \times [-1.0 \times 10^{-10}, 1.0 \times 10^{-10}]$. (For interpretation of the references to color in this figure legend, the reader is referred to the web version of this article.)

the escapes are evenly distributed between both the bottom and top exits. As I_{esc} increases, there is a tendency for the particles to escape through the bottom exit, more prominently for $\varepsilon = 1.0 \times 10^{-3}$ [Fig. 6(a)], characterizing the ratchet effect.

According to Gong and Brumer [44], the average of I over an ensemble of initial conditions, $\langle I \rangle$, represents the net current and the ratchet effect can also be characterized by a nonzero mean action. Thus, we calculate the average of the action as a function of time for the same previously used ensemble of 10^6 randomly chosen initial conditions for the same three distinct values of ε used in Fig. 6 [Fig. 7(a)]. We observe a nonzero net current for all three cases for times $n > 10^2$. The mean value of I increases with ε because the volume of the chaotic component is larger for larger ε.

Therefore, we have enough numerical evidence to state that the Hamiltonian nontwist mapping, given by Eq. (4), exhibits the Hamiltonian ratchet effect. To understand the cause of this directed transport, we consider a single chaotic initial condition, $(\theta, I) = (0.5, 1.0 \times 10^{-10})$, and iterate it for $N = 10^9$ times with $\varepsilon = 1.0 \times 10^{-3}$, $\varepsilon = 2.0 \times 10^{-3}$, and $\varepsilon = 3.0 \times 10^{-3}$. We count the time it spends in both upper ($I > 0$) and lower ($I < 0$) regions of phase space. From this, we obtain two collections of recurrence times $\{t_j^{(U)}\}_{j=1,2,\ldots,\mathcal{N}^{(U)}}$ and $\{t_j^{(L)}\}_{j=1,2,\ldots,\mathcal{N}^{(L)}}$,

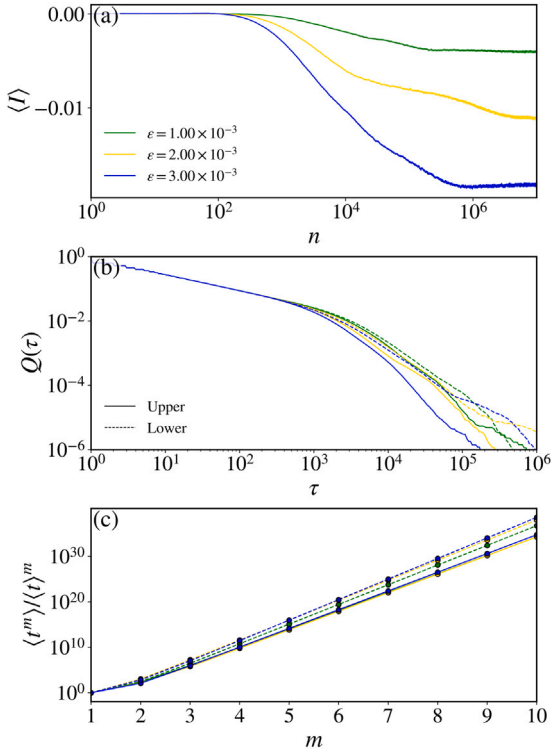

Fig. 7. (a) The average of the action for an ensemble of $M = 10^6$ initial conditions randomly distributed on $I = 1.0 \times 10^{-10}$ at $n = 0$ for (green) $\varepsilon = 1.0 \times 10^{-3}$, (yellow) $\varepsilon = 2.0 \times 10^{-3}$, and (blue) $\varepsilon = 3.0 \times 10^{-3}$. (b) The cumulative distribution of recurrence times for the (full lines) top ($I > 0$) and (dashed lines) bottom ($I < 0$) regions of phase space. (c) Moments of the distribution of recurrence times normalized to $\langle t \rangle$. (For interpretation of the references to color in this figure legend, the reader is referred to the web version of this article.)

where $\mathcal{N}^{(U)}$ and $\mathcal{N}^{(L)}$ are the total number of recurrence times for the upper and lower regions, respectively,[1] and define the probability distribution of recurrence times as $P^{(U,L)}(t)$ for both collections of recurrence times. Alternatively, we define the cumulative distribution of recurrence times, $Q^{(U,L)}(\tau)$, as follows:

$$Q^{(U,L)}(\tau) = \sum_{t>\tau} P^{(U,L)}(t) = \frac{M^{(U,L)}}{\mathcal{N}^{(U,L)}}, \tag{9}$$

where $M^{(U,L)}$ is the number of recurrence times larger than τ, *i.e.*, the number of occurrences where $t > \tau$, for the respective regions with $\tau \in [1, 2, \ldots, t_{max}]$, where t_{max} is the largest recurrence time detected. Fig. 7(b) shows the cumulative distribution of recurrence times for the three values of ε mentioned above for both collections of recurrence times, where the full lines correspond to the upper region while the dashed lines to the lower one. We observe a power law tail for larger τ, characteristic of systems that exhibit the stickiness effect [19–24]. Furthermore, we observe different distributions for the upper and lower recurrence regions [full and dashed lines, respectively, in Fig. 7(b)]: the decay is faster for the upper region. The difference between these two distributions becomes more evident when we calculate the higher moments of $P(t)$:

$$\langle t^m \rangle = \int_0^{t_{max}} t^m P(t)\, dt\,. \tag{10}$$

In Fig. 7(c) we show the moments up to $m = 10$ normalized to $\langle t \rangle$. Starting from $m = 2$, the difference in the moments of the upper

[1] For the mentioned number of iterations, we obtained $\mathcal{N} \sim 10^6$ for all values of ε.

Table 3
The first moment, *i.e.*, the mean recurrence time, of the recurrence time distributions for different values of ε for the upper and lower regions of phase space.

ε	$\langle t\rangle^{(\mathrm{U})}$	$\langle t\rangle^{(\mathrm{L})}$	$\langle t\rangle^{(\mathrm{L})} - \langle t\rangle^{(\mathrm{U})}$
1.0×10^{-3}	1.31×10^{2}	1.51×10^{2}	0.20×10^{2}
2.0×10^{-3}	1.02×10^{2}	1.33×10^{2}	0.31×10^{2}
3.0×10^{-3}	0.83×10^{2}	1.21×10^{2}	0.38×10^{2}

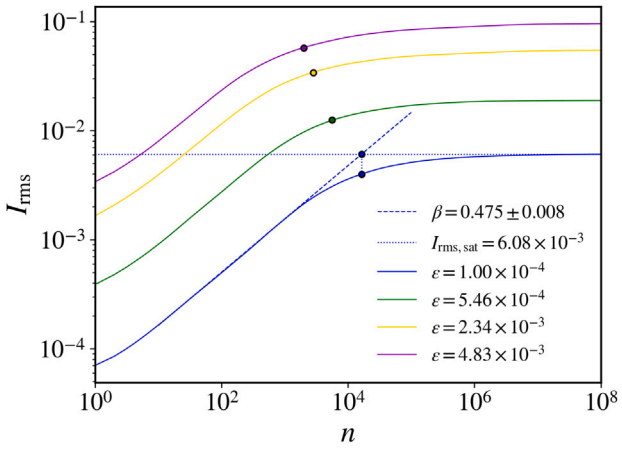

Fig. 8. The I_{rms} as a function of the number of iterations for four distinct values of the perturbation ε. The colored dots indicate the transition point from the growth regime to the constant plateau of saturation. These points are determined by the intersection of the line obtained from the fitting of I_{rms} versus n in the growth regime and the horizontal line $I_{\mathrm{rms}} = I_{\mathrm{rms,sat}}$. (For interpretation of the references to color in this figure legend, the reader is referred to the web version of this article.)

and lower distributions is already noticeable. Moreover, there is a substantial difference in the first moments as well (Table 3).

Therefore, the difference in the upper and lower distribution is evidence of an unbalanced stickiness in phase space. This phenomenon makes chaotic orbits to stick in the upper and lower region of phase space unevenly due to the spatial asymmetry with respect to the $I = 0$ line, creating the directed transport. Similar results have been reported in Ref. [62] for the extended standard nontwist map. It is important to emphasize, however, that it is the existence of asymmetric islands that leads to such a phenomenon, *i.e.*, there is no symmetry transformation between the upper and lower islands. Additionally, the perturbation ε and the survival region also influence the transport (Fig. 6). In regions without stability islands, the particles escape evenly from the bottom and top exits.

4. Critical exponents and scaling law

In this section, we analyze the diffusion of chaotic orbits in phase space and the scaling properties of the chaotic component of phase space. We use the square root of the averaged squared action, defined as

$$I_{\mathrm{rms}} = \sqrt{\frac{1}{M}\sum_{i=1}^{M}\frac{1}{n}\sum_{j=1}^{n} I_{i,j}^{2}}, \tag{11}$$

where M corresponds to an ensemble of initial conditions and n is the length of the time series, as our observable.

The behavior of I_{rms} is shown in Fig. 8 for different perturbation values ε. The curves exhibit an accelerated growth regime for small n whereas for large n, they achieve a saturation limit, characterized by a constant plateau due to the bounded phase space area. The transition from accelerated growth to the constant plateau is given by a characteristic crossover number n_x. The behavior discussed above can be characterized by four critical exponents, namely, α, β, γ, and z. To obtain them, we assume the following scaling hypotheses [81,95–100]

1. For times $n \ll n_x$, I_{rms} scales as
$$I_{\mathrm{rms}} \sim (n\varepsilon^{\alpha})^{\beta}, \tag{12}$$
where α is the transport exponent and β corresponds to the acceleration exponent.
2. For $n \gg n_x$ the curve saturates, and the saturation value depends on ε as
$$I_{\mathrm{rms,sat}} \sim \varepsilon^{\gamma}, \tag{13}$$
where γ is the saturation exponent.
3. Finally, there is a changeover from an accelerated regime of growth to a constant plateau, identified by the crossover number n_x and
$$n_x \sim \varepsilon^{z}, \tag{14}$$
where z is the crossover exponent.

Therefore, using these scaling hypotheses, we describe the behavior of I_{rms} by a generalized homogeneous function, given by [95–97]

$$I_{\mathrm{rms}}(n\varepsilon^{\alpha}, \varepsilon) = \ell\, I_{\mathrm{rms}}(\ell^{a} n\varepsilon^{\alpha}, \ell^{b}\varepsilon), \tag{15}$$

where ℓ is a scaling factor and a and b are characteristic exponents. It is convenient to set $\ell^{a} n\varepsilon^{\alpha} = 1$, leading us to

$$\ell = (n\varepsilon^{\alpha})^{-1/a}. \tag{16}$$

By substituting Eq. (16) into Eq. (15), we obtain

$$I_{\mathrm{rms}}(n\varepsilon^{\alpha}, \varepsilon) = (n\varepsilon^{\alpha})^{-1/a} I_{\mathrm{rms}}(1, (n\varepsilon^{\alpha})^{-b/a}\varepsilon). \tag{17}$$

We assume $I_{\mathrm{rms}}(1, (n\varepsilon^{\alpha})^{-b/a}\varepsilon) = \text{const}$ for $n \ll n_x$, and comparing Eq. (17) with the first scaling hypothesis, Eq. (12), we find $a = -1/\beta$.

Analogously, we set $\ell^{b}\varepsilon = 1$ and obtain

$$\ell = \varepsilon^{-1/b}. \tag{18}$$

Using Eq. (18), we can rewrite Eq. (15) as

$$I_{\mathrm{rms}}(n\varepsilon^{\alpha}, \varepsilon) = \varepsilon^{-1/b} I_{\mathrm{rms}}(\varepsilon^{-a/b} n\varepsilon^{\alpha}, 1), \tag{19}$$

where $I_{\mathrm{rms}}(\varepsilon^{-a/b} n\varepsilon^{\alpha}, 1)$ is assumed to be constant for $n \gg n_x$ (saturation regime). Therefore, upon comparing Eqs. (19) and the second scaling hypothesis, Eq. (13), we find $b = -1/\gamma$.

Therefore, the critical exponent z can be obtained by combining the two scaling factors, Eqs. (16) and (18), together with the values of a and b we have just found, at the transition point $n = n_x$. Indeed, we obtain

$$n_x = \varepsilon^{\frac{\gamma}{\beta} - \alpha}. \tag{20}$$

Finally, by comparing Eq. (20) with the third scaling hypothesis, Eq. (14), we obtain the following scaling law

$$z = \frac{\gamma}{\beta} - \alpha. \tag{21}$$

Through numerical simulations, we obtain all these exponents. The acceleration exponent β is obtained by plotting I_{rms} versus n (Fig. 8) and performing a power law fitting $f(n) = Bn^{A}$ over the regime of growth. The exponent β brings important information about diffusion. If $\beta = 0.5$, normal diffusion dominates the dynamics. Exponents larger (smaller) than 0.5 means super (sub) diffusion. We find that the exponent β corresponds to A, and equals $\beta = 0.475 \pm 0.008$,[2] slightly less than 0.5, meaning the diffusion process is sub diffusive. From the same power law fitting, we find $B = \varepsilon^{\alpha\beta}$. From different values of ε we obtain different values of B and from a power law fitting of B versus

[2] We performed the power law fitting for several values of ε (those indicated in Fig. 9) and this value corresponds to $\langle\beta\rangle \pm \sigma_{\beta}$, where $\langle\cdot\rangle$ is the mean and σ_{β} is the standard deviation.

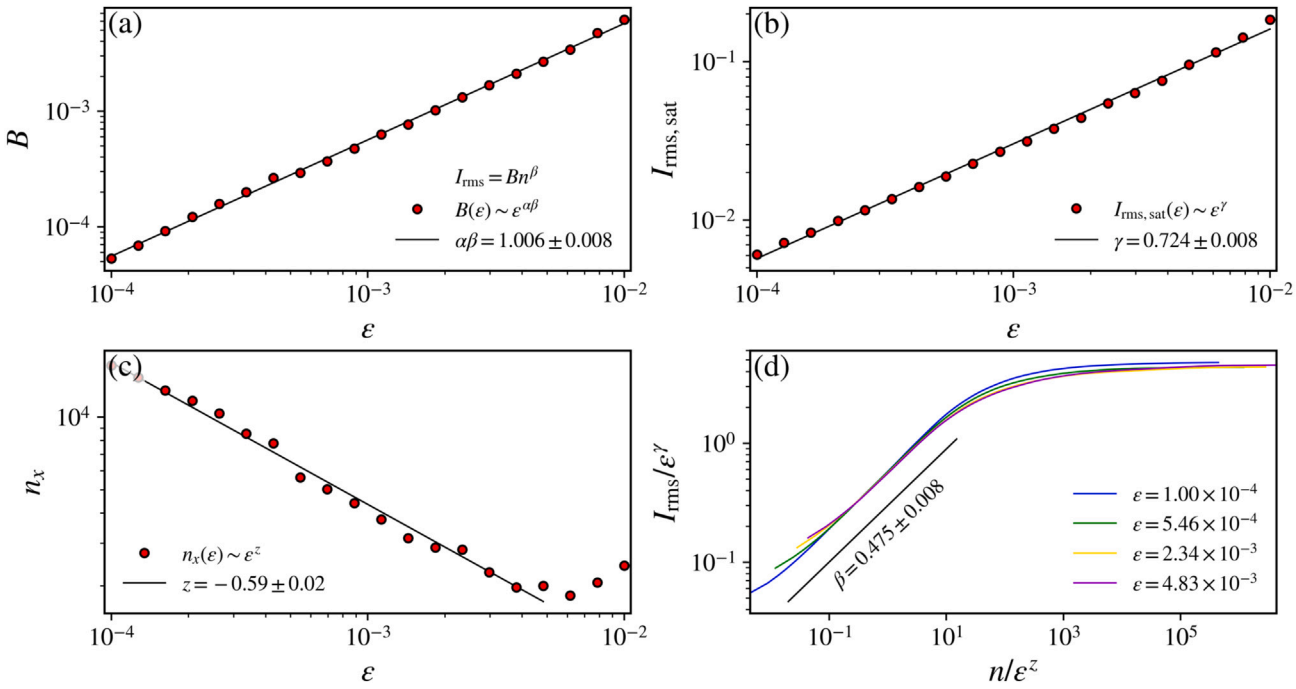

Fig. 9. (a) The exponent $B(\varepsilon)$ from the power law fitting of I_{rms} versus n (Fig. 8), $I_{rms} = Bn^{\beta}$ as a function of ε. It scales with ε as $B \sim \varepsilon^{\alpha\beta}$, and from the optimal fitting we obtain $\alpha\beta = 1.006 \pm 0.008$. (b) The saturation value of I_{rms}, $I_{rms,sat}$ as a function of ε. The saturation value is obtained for $n \gg n_x$ and it scales as a power law, with exponent $\gamma = 0.724 \pm 0.008$. (c) The transition point, n_x, from the growth regime to the constant plateau of saturation (colored dots in Fig. 8) as a function of ε. It depends on ε as a power law, and from the optimal fitting we obtain for the crossover exponent $z = -0.59 \pm 0.02$. (d) The overlap of all curves in Fig. 8 onto a single, and hence, universal curve after the transformations $n \to n/\varepsilon^{z}$ and $I_{rms} \to I_{rms}/\varepsilon^{\gamma}$.

ε [Fig. 9(a)], we obtain $\alpha\beta = 1.009 \pm 0.009$, such that the transport exponent is $\alpha = 2.12 \pm 0.05$.

The saturation exponent, γ, is obtained using the second scaling hypothesis, Eq. (13). We plot the saturation point of I_{rms}, $I_{rms,sat}$, as a function of ε and perform a power law fitting [Fig. 9(b)] to obtain $\gamma = 0.724 \pm 0.008$. As for the crossover exponent, z, defined by the third scaling hypothesis, Eq. (14), we plot the point n_x that marks the transition from a growth regime to the constant plateau of saturation observed in Fig. 8 as a function of ε [Fig. 9(c)]. These points are indicated as colored dots in Fig. 8. Through a power law fitting, we obtain $z = -0.59 \pm 0.02$. Instead of performing the last mentioned power law fitting to find z, we could use the scaling law, given by Eq. (21), to obtain z given α, β, and γ. We obtain, in this case, $z = -0.6 \pm 0.1$, which remarkably agrees with the value obtained numerically, with a larger uncertainty, however. Furthermore, under the transformations $n \to n\varepsilon^{z}$, $I_{rms} \to I_{rms}/\varepsilon^{\gamma}$, the curves I_{rms} versus n for different ε overlap onto a single, and hence, universal curve [Fig. 9(d)], confirming, therefore, the scaling invariance in the chaotic component of phase space.

Let us now discuss our first scaling hypothesis, Eq. (12). We have assumed that I_{esc} scales with the perturbation ε with an exponent of $\alpha\beta$. In several other works, the transport exponent has been assumed $\alpha = 2$ *ad hoc* to validate the scaling assumptions [81,95–100], given that the acceleration exponent is $\beta = 0.5$, resulting in $\alpha\beta = 1$, for these cases. In a more recent work, Leonel et al. [84] demonstrated analytically the presence of the term ε^2 for the Leonel mapping. This leads to $\beta = 0.5$ in order to satisfy $\alpha\beta = 1$. Here, instead of assuming *a priori* a value for α or for the product $\alpha\beta$, we have proposed a more general scaling hypothesis [Eq. (12)] with which we have numerically obtained $\alpha\beta = 1$ (within numerical errors). In our case, the acceleration exponent slightly deviates from the value for the Leonel mapping, namely, $\beta = 0.475 \pm 0.008$, resulting in a transport exponent of $\alpha = 2.12 \pm 0.05$.

5. Conclusions

The $\mathbf{E} \times \mathbf{B}$ drift motion is observed in many plasma devices and plays a major role in the anomalous transport of particles. In magnetic confinement devices, $\mathbf{E} \times \mathbf{B}$ shear is responsible for reducing turbulence levels, improving the confinement. Thus, understanding this drift motion is crucial for improving plasma confinement and optimizing various applications. In this paper, we have explored the transport and diffusion of particles in the chaotic component in phase space in a newly reported nontwist Hamiltonian mapping, that describes the advected particle motion under the $\mathbf{E} \times \mathbf{B}$ drift. Firstly, our analysis focused on the properties of the survival probability considering two exits symmetrically placed on phase space with respect to the $I = 0$ line. We have demonstrated that the survival probability follows an exponential decay when the chaotic sea dominates the survival region. For survival region defined with $I_{esc} > I_{fi}$, where I_{fi} is the center of the elliptical fixed point of the first period-1 island, the survival probability follows a stretched exponential with a power law tail for long times. Furthermore, we have shown that the decay rate scales with I_{esc} as a power law for $I_{esc} < I_{fi}$, with exponent $\zeta = -1.865 \pm 0.007$. By rescaling the horizontal axis of the plot $P(n) \times n$ by $n \to nI_{esc}^{\zeta}$, we have found that the survival probability curves overlap into a single, and hence universal, plot for small survival regions, indicating that the survival probability maintains its behavior regardless of the size of the survival region.

Secondly, we investigated whether the chaotic transport of particles has a preferential direction, *i.e.*, whether the system exhibits unbiased transport. We have shown that considering particles distributed uniformly over the whole available phase space or particles randomly distributed over a small region around $I = 0$, both ensembles initially with $\langle I \rangle \approx 0$, the tendency is for the particles to escape through the bottom exit, thus exhibiting the so-called ratchet effect. The mechanics responsible for this effect is an unbalanced stickiness due to asymmetry of the chaotic component in phase space with respect to the line $I = 0$, *i.e.*, the invariant spanning curves that bound the phase space are not symmetrical. This asymmetry generates a nonzero net current of particles due to different trapping times in the upper ($I > 0$) and lower ($I < 0$) regions of phase space. The cumulative distribution of recurrence times and the difference in the moments of the distribution of

recurrence times support our claim for the existence of an unbalanced stickiness in phase space. To the best of our knowledge, the existence of a ratchet current in the $\mathbf{E} \times \mathbf{B}$ drift motion has not been reported in the literature. This fact has complex implications for the impurity transport, heating, and instabilities in the plasma, and future studies are necessary to better understand them.

Lastly, we presented a phenomenological description of diffusion in the chaotic component of phase space. We have chosen as our observable the square root of the averaged square action, I_{rms}, and upon assuming three scaling hypotheses, we have found that the behavior of I_{rms} is characterized by four critical exponents. One of the exponents, β, characterizes the diffusion process. We have obtained $\beta = 0.475 \pm 0.008$, which is slightly below 0.5, indicating that the diffusion process is subdiffusive. The subdiffusive nature of the system is related to the trappings that generate the stickiness effect a chaotic orbit experiences throughout its evolution [101]. We have also derived an analytical scaling law relating these four exponents and from extensive numerical simulations, we have obtained all of them and showed that they remarkably agree with the scaling law. Our scaling hypotheses were supported by the collapse of the I_{rms} curves onto a single, and hence universal, curve. Additionally, even though the obtained scaling law [Eq. (21)] is similar to the Family-Vicsek scaling discussed in Ref. [102], it is not directly connected. Nonetheless, this similarity motivates us to explore whether there is a correlation length that reaches the size of the bounded phase space area in the saturation regime. We intend to investigate this in a forthcoming paper.

Code availability

The source code to reproduce the results reported in this paper is freely available on the Zenodo archive [103] and in the GitHub repository [104].

CRediT authorship contribution statement

Matheus Rolim Sales: Writing – review & editing, Writing – original draft, Visualization, Validation, Software, Methodology, Investigation, Formal analysis, Data curation, Conceptualization. **Daniel Borin:** Writing – review & editing, Writing – original draft, Visualization, Validation, Methodology, Investigation, Formal analysis, Data curation, Conceptualization. **Leonardo Costa de Souza:** Writing – review & editing, Writing – original draft, Visualization, Validation, Methodology, Investigation, Formal analysis, Data curation, Conceptualization. **José Danilo Szezech Jr.:** Writing – review & editing, Writing – original draft, Visualization, Validation, Methodology, Investigation, Formal analysis, Data curation, Conceptualization. **Ricardo Luiz Viana:** Writing – review & editing, Writing – original draft, Visualization, Validation, Methodology, Investigation, Formal analysis, Data curation, Conceptualization. **Iberê Luiz Caldas:** Writing – review & editing, Writing – original draft, Visualization, Validation, Methodology, Investigation, Formal analysis, Data curation, Conceptualization. **Edson Denis Leonel:** Writing – review & editing, Writing – original draft, Visualization, Validation, Methodology, Investigation, Formal analysis, Data curation, Conceptualization.

Declaration of competing interest

The authors declare that they have no known competing financial interests or personal relationships that could have appeared to influence the work reported in this paper.

Data availability

I have shared the source code to reproduce the results in Zenodo and GitHub.

Acknowledgments

This work was supported by the Araucária Foundation, Brazil, the Coordination of Superior Level Staff Improvement (CAPES), Brazil, the National Council for Scientific and Technological Development (CNPq), Brazil, under Grant Nos. 01318/2019-0, 301019/2019-3, 403120/2021-7, 309670/2023-3, and by the São Paulo Research Foundation, Brazil, under Grant Nos. 2018/03211-6, 2019/14038-6, 2022/03612-6, 2023/08698-9, 2023/16146-6.

References

[1] Lichtenberg AJ, Lieberman MA. Regular and chaotic dynamics. Applied mathematical sciences, vol. 38, Springer-Verlag; 1992.
[2] Mackay RS, Meiss JD, Percival IC. Transport in Hamiltonian systems. Physica D 1984;13(1):55–81. http://dx.doi.org/10.1016/0167-2789(84)90270-7, URL https://www.sciencedirect.com/science/article/pii/0167278984902707.
[3] MacKay RS, Meiss JD, Percival IC. Stochasticity and transport in Hamiltonian systems. Phys Rev Lett 1984;52:697–700. http://dx.doi.org/10.1103/PhysRevLett.52.697, URL https://link.aps.org/doi/10.1103/PhysRevLett.52.697.
[4] Efthymiopoulos C, Contopoulos G, Voglis N, Dvorak R. Stickiness and cantori. J Phys A: Math Gen 1997;30(23):8167. http://dx.doi.org/10.1088/0305-4470/30/23/016.
[5] Contopoulos G. Orbits in highly perturbed dynamical systems. iii. nonperiodic orbits. Astron J 1971;76:147. http://dx.doi.org/10.1086/111098, URL https://ui.adsabs.harvard.edu/abs/1971AJ..76.147C.
[6] Karney CF. Long-time correlations in the stochastic regime. Physica D 1983;8(3):360–80. http://dx.doi.org/10.1016/0167-2789(83)90232-4, URL https://www.sciencedirect.com/science/article/pii/0167278983902324.
[7] Meiss JD, Cary JR, Grebogi C, Crawford JD, Kaufman AN, Abarbanel HD. Correlations of periodic, area-preserving maps. Physica D 1983;6(3):375–84. http://dx.doi.org/10.1016/0167-2789(83)90019-2, URL https://www.sciencedirect.com/science/article/pii/0167278983900192.
[8] Chirikov B, Shepelyansky D. Correlation properties of dynamical chaos in Hamiltonian systems. Physica D 1984;13(3):395–400. http://dx.doi.org/10.1016/0167-2789(84)90140-4, URL https://www.sciencedirect.com/science/article/pii/0167278984901404.
[9] Contopoulos G, Harsoula M. Stickiness in chaos. Int J Bifurcation Chaos 2008;18(10):2929–49. http://dx.doi.org/10.1142/S0218127408022172.
[10] Cristadoro G, Ketzmerick R. Universality of algebraic decays in Hamiltonian systems. Phys Rev Lett 2008;100:184101. http://dx.doi.org/10.1103/PhysRevLett.100.184101, URL https://link.aps.org/doi/10.1103/PhysRevLett.100.184101.
[11] Contopoulos G, Harsoula M. Stickiness effects in conservative systems. Int J Bifurcation Chaos 2010;20(07):2005–43. http://dx.doi.org/10.1142/S0218127410026915.
[12] Zaslavsky G. Dynamical traps. Physica D 2002;168–169:292–304. http://dx.doi.org/10.1016/S0167-2789(02)00516-X, URL https://www.sciencedirect.com/science/article/pii/S016727890200516X.
[13] Meiss JD, Ott E. Markov-tree model of intrinsic transport in Hamiltonian systems. Phys Rev Lett 1985;55:2741–4. http://dx.doi.org/10.1103/PhysRevLett.55.2741, URL https://link.aps.org/doi/10.1103/PhysRevLett.55.2741.
[14] Meiss JD, Ott E. Markov tree model of transport in area-preserving maps. Physica D 1986;20(2):387–402. http://dx.doi.org/10.1016/0167-2789(86)90041-2, URL https://www.sciencedirect.com/science/article/pii/0167278986900412.
[15] Zaslavskiĭ GM, Chirikov BV. Stochastic instability of non-linear oscillations. Sov Phys Uspekhi 1972;14(5):549. http://dx.doi.org/10.1070/PU1972v014n05ABEH004669.
[16] Zaslavsky GM, Edelman M, Niyazov BA. Self-similarity, renormalization, and phase space nonuniformity of Hamiltonian chaotic dynamics. Chaos 1997;7(1):159–81. http://dx.doi.org/10.1063/1.166252.
[17] Zaslavsky G. Chaos, fractional kinetics, and anomalous transport. Phys Rep 2002;371(6):461–580. http://dx.doi.org/10.1016/S0370-1573(02)00331-9, URL https://www.sciencedirect.com/science/article/pii/S0370157302003319.
[18] Zaslavsky GM. Hamiltonian chaos and fractional dynamics. USA: Oxford University Press; 2005.
[19] Afraimovich V, Zaslavsky GM. Fractal and multifractal properties of exit times and Poincarérecurrences. Phys Rev E 1997;55:5418–26. http://dx.doi.org/10.1103/PhysRevE.55.5418, URL https://link.aps.org/doi/10.1103/PhysRevE.55.5418.
[20] Altmann EG, Motter AE, Kantz H. Stickiness in mushroom billiards. Chaos 2005;15(3):033105. http://dx.doi.org/10.1063/1.1979211.
[21] Altmann EG, Motter AE, Kantz H. Stickiness in hamiltonian systems: From sharply divided to hierarchical phase space. Phys Rev E 2006;73:026207. http://dx.doi.org/10.1103/PhysRevE.73.026207, URL https://link.aps.org/doi/10.1103/PhysRevE.73.026207.

[22] Venegeroles R. Universality of algebraic laws in Hamiltonian systems. Phys Rev Lett 2009;102:064101. http://dx.doi.org/10.1103/PhysRevLett.102.064101, URL https://link.aps.org/doi/10.1103/PhysRevLett.102.064101.

[23] Abud CV, de Carvalho RE. Multifractality, stickiness, and recurrence-time statistics. Phys Rev E 2013;88:042922. http://dx.doi.org/10.1103/PhysRevE.88.042922, URL https://link.aps.org/doi/10.1103/PhysRevE.88.042922.

[24] Lozej Č. Stickiness in generic low-dimensional Hamiltonian systems: A recurrence-time statistics approach. Phys Rev E 2020;101:052204. http://dx.doi.org/10.1103/PhysRevE.101.052204, URL https://link.aps.org/doi/10.1103/PhysRevE.101.052204.

[25] Lai Y-C, Ding M, Grebogi C, Blümel R. Algebraic decay and fluctuations of the decay exponent in Hamiltonian systems. Phys Rev A 1992;46:4661–9. http://dx.doi.org/10.1103/PhysRevA.46.4661, URL https://link.aps.org/doi/10.1103/PhysRevA.46.4661.

[26] Altmann EG, Tél T. Poincaré recurrences and transient chaos in systems with leaks. Phys Rev E 2009;79:016204. http://dx.doi.org/10.1103/PhysRevE.79.016204, URL https://link.aps.org/doi/10.1103/PhysRevE.79.016204.

[27] Avetisov VA, Nechaev SK. Chaotic hamiltonian systems: Survival probability. Phys Rev E 2010;81:046211. http://dx.doi.org/10.1103/PhysRevE.81.046211, URL https://link.aps.org/doi/10.1103/PhysRevE.81.046211.

[28] Dettmann CP, Leonel ED. Escape and transport for an open bouncer: Stretched exponential decays. Physica D 2012;241(4):403–8. http://dx.doi.org/10.1016/j.physd.2011.10.012, URL https://www.sciencedirect.com/science/article/pii/S0167278911002910.

[29] Leonel ED, Dettmann CP. Recurrence of particles in static and time varying oval billiards. Phys Lett A 2012;376(20):1669–74. http://dx.doi.org/10.1016/j.physleta.2012.03.056, URL https://www.sciencedirect.com/science/article/pii/S0375960112004045.

[30] Livorati ALP, Kroetz T, Dettmann CP, Caldas IL, Leonel ED. Stickiness in a bouncer model: A slowing mechanism for Fermi acceleration. Phys Rev E 2012;86:036203. http://dx.doi.org/10.1103/PhysRevE.86.036203, URL https://link.aps.org/doi/10.1103/PhysRevE.86.036203.

[31] Livorati ALP, Georgiou O, Dettmann CP, Leonel ED. Escape through a time-dependent hole in the doubling map. Phys Rev E 2014;89:052913. http://dx.doi.org/10.1103/PhysRevE.89.052913, URL https://link.aps.org/doi/10.1103/PhysRevE.89.052913.

[32] Méndez-Bermúdez JA, Martínez-Mendoza AJ, Livorati ALP, Leonel ED. Leaking of trajectories from the phase space of discontinuous dynamics. J Phys A 2015;48(40):405101. http://dx.doi.org/10.1088/1751-8113/48/40/405101.

[33] de Faria NB, Tavares DS, de Paula WCS, Leonel ED, Ladeira DG. Transport of chaotic trajectories from regions distant from or near to structures of regular motion of the Fermi-Ulam model. Phys Rev E 2016;94:042208. http://dx.doi.org/10.1103/PhysRevE.94.042208, URL https://link.aps.org/doi/10.1103/PhysRevE.94.042208.

[34] Livorati AL, Palmero MS, Díaz-I G, Dettmann CP, Caldas IL, Leonel ED. Investigation of stickiness influence in the anomalous transport and diffusion for a non-dissipative Fermi–Ulam model. Commun Nonlinear Sci Numer Simul 2018;55:225–36. http://dx.doi.org/10.1016/j.cnsns.2017.07.010, URL https://www.sciencedirect.com/science/article/pii/S1007570417302605.

[35] Borin D, Livorati ALP, Leonel ED. An investigation of the survival probability for chaotic diffusion in a family of discrete Hamiltonian mappings. Chaos Solitons Fractals 2023;175:113965. http://dx.doi.org/10.1016/j.chaos.2023.113965, URL https://www.sciencedirect.com/science/article/pii/S0960077923008664.

[36] Vivaldi F, Casati G, Guarneri I. Origin of long-time tails in strongly chaotic systems. Phys Rev Lett 1983;51:727–30. http://dx.doi.org/10.1103/PhysRevLett.51.727, URL https://link.aps.org/doi/10.1103/PhysRevLett.51.727.

[37] Lozej Č, Robnik M. Structure, size, and statistical properties of chaotic components in a mixed-type Hamiltonian system. Phys Rev E 2018;98:022220. http://dx.doi.org/10.1103/PhysRevE.98.022220, URL https://link.aps.org/doi/10.1103/PhysRevE.98.022220.

[38] Dittrich T, Ketzmerick R, Otto M-F, Schanz H. Classical and quantum transport in deterministic Hamiltonian ratchets. Ann Phys, Lpz 2000;512(9–10):755–63. http://dx.doi.org/10.1002/andp.200051209-1011, URL https://onlinelibrary.wiley.com/doi/abs/10.1002/andp.200051209-1011.

[39] Denisov S, Flach S. Dynamical mechanisms of dc current generation in driven Hamiltonian systems. Phys Rev E 2001;64:056236. http://dx.doi.org/10.1103/PhysRevE.64.056236, URL https://link.aps.org/doi/10.1103/PhysRevE.64.056236.

[40] Schanz H, Otto M-F, Ketzmerick R, Dittrich T. Classical and quantum Hamiltonian ratchets. Phys Rev Lett 2001;87:070601. http://dx.doi.org/10.1103/PhysRevLett.87.070601, URL https://link.aps.org/doi/10.1103/PhysRevLett.87.070601.

[41] Denisov S, Klafter J, Urbakh M, Flach S. Dc currents in Hamiltonian systems by lévy flights. Physica D 2002;170(2):131–42. http://dx.doi.org/10.1016/S0167-2789(02)00545-6, URL https://www.sciencedirect.com/science/article/pii/S0167278902005456.

[42] Monteiro TS, Dando PA, Hutchings NAC, Isherwood MR. Proposal for a chaotic ratchet using cold atoms in optical lattices. Phys Rev Lett 2002;89:194102. http://dx.doi.org/10.1103/PhysRevLett.89.194102, URL https://link.aps.org/doi/10.1103/PhysRevLett.89.194102.

[43] Cheon T, Exner P, Šeba P. Extended standard map with spatio-temporal asymmetry. J Phys Soc Japan 2003;72(5):1087–91. http://dx.doi.org/10.1143/JPSJ.72.1087.

[44] Gong J, Brumer P. Directed anomalous diffusion without a biased field: A ratchet accelerator. Phys Rev E 2004;70:016202. http://dx.doi.org/10.1103/PhysRevE.70.016202, URL https://link.aps.org/doi/10.1103/PhysRevE.70.016202.

[45] Abrikosov AA. Fundamentals of the theory of metals. Courier Dover Publications; 2017, URL https://books.google.com.br/books?hl=pt-BR&lr=&id=SM02DwAAQBAJ&oi=fnd&pg=PR5&dq=+Fundamentals+of+the+Theory+of+Metals&ots=24WbW4jj5l&sig=weKxMztDEzwwLbrNPBoCtdSHe84#v=onepage&q=Fundamentals%20of%20the%20Theory%20of%20Metals&f=false.

[46] Zapata I, Bartussek R, Sols F, Hänggi P. Voltage rectification by a SQUID ratchet. Phys Rev Lett 1996;77:2292–5. http://dx.doi.org/10.1103/PhysRevLett.77.2292, URL https://link.aps.org/doi/10.1103/PhysRevLett.77.2292.

[47] Reimann P. Brownian motors: Noisy transport far from equilibrium. Phys Rep 2002;361(2–4):57–265. http://dx.doi.org/10.1016/S0370-1573(01)00081-3.

[48] Jülicher F, Ajdari A, Prost J. Modeling molecular motors. Rev Modern Phys 1997;69:1269–82. http://dx.doi.org/10.1103/RevModPhys.69.1269, URL https://link.aps.org/doi/10.1103/RevModPhys.69.1269.

[49] Moore FL, Robinson JC, Bharucha CF, Sundaram B, Raizen MG. Atom optics realization of the quantum δ-kicked rotor. Phys Rev Lett 1995;75:4598–601. http://dx.doi.org/10.1103/PhysRevLett.75.4598, URL https://link.aps.org/doi/10.1103/PhysRevLett.75.4598.

[50] Robinson JC, Bharucha CF, Madison KW, Moore FL, Sundaram B, Wilkinson SR, Raizen MG. Can a single-pulse standing wave induce chaos in atomic motion? Phys Rev Lett 1996;76:3304–7. http://dx.doi.org/10.1103/PhysRevLett.76.3304, URL https://link.aps.org/doi/10.1103/PhysRevLett.76.3304.

[51] Mennerat-Robilliard C, Lucas D, Guibal S, Tabosa J, Jurczak C, Courtois J-Y, Grynberg G. Ratchet for cold rubidium atoms: The asymmetric optical lattice. Phys Rev Lett 1999;82:851–4. http://dx.doi.org/10.1103/PhysRevLett.82.851, URL https://link.aps.org/doi/10.1103/PhysRevLett.82.851.

[52] Monteiro TS, Dando PA, Hutchings NAC, Isherwood MR. Proposal for a chaotic ratchet using cold atoms in optical lattices. Phys Rev Lett 2002;89(19):194102. http://dx.doi.org/10.1103/PhysRevLett.89.194102, URL https://link.aps.org/doi/10.1103/PhysRevLett.89.194102.

[53] Bass FG, Bulgakov AA. Kinetic and electrodynamic phenomena in classical and quantum semiconductor superlattices. Nova Publishers; 1997, URL https://books.google.com.br/books?hl=pt-BR&lr=&id=BVnqz_0HXMsC&oi=fnd&pg=PA7&dq=F.+G.+Bass+and+A.+Bulgakov,Kinetic+and+Electrodynamic+Phenomena+in+Classical+and+Quantum+Semiconductor+Superlattices+(Nova+Science+Publishing,+Commack,+NY,+1997).&ots=dQJH6zlKN8&sig=ZIOnb3RcMHTz6uEGcK1fNxSfXbQ#v=onepage&q&f=false.

[54] Schelin AB, Spatschek KH. Directed chaotic transport in the tokamap with mixed phase space. Phys Rev E 2010;81:016205. http://dx.doi.org/10.1103/PhysRevE.81.016205, URL https://link.aps.org/doi/10.1103/PhysRevE.81.016205.

[55] Bartussek R, Hänggi P, Kissner JG. Periodically rocked thermal ratchets. Europhys Lett 1994;28(7):459. http://dx.doi.org/10.1209/0295-5075/28/7/001.

[56] Łuczka J, Czernik T, Hänggi P. Symmetric white noise can induce directed current in ratchets. Phys Rev E 1997;56:3968–75. http://dx.doi.org/10.1103/PhysRevE.56.3968, URL https://link.aps.org/doi/10.1103/PhysRevE.56.3968.

[57] Jung P, Kissner JG, Hänggi P. Regular and chaotic transport in asymmetric periodic potentials: Inertia ratchets. Phys Rev Lett 1996;76:3436–9. http://dx.doi.org/10.1103/PhysRevLett.76.3436, URL https://link.aps.org/doi/10.1103/PhysRevLett.76.3436.

[58] Flach S, Yevtushenko O, Zolotaryuk Y. Directed current due to broken time-space symmetry. Phys Rev Lett 2000;84:2358–61. http://dx.doi.org/10.1103/PhysRevLett.84.2358, URL https://link.aps.org/doi/10.1103/PhysRevLett.84.2358.

[59] Mateos JL. Chaotic transport and current reversal in deterministic ratchets. Phys Rev Lett 2000;84:258–61. http://dx.doi.org/10.1103/PhysRevLett.84.258, URL https://link.aps.org/doi/10.1103/PhysRevLett.84.258.

[60] Porto M, Urbakh M, Klafter J. Molecular motor that never steps backwards. Phys Rev Lett 2000;85:491–4. http://dx.doi.org/10.1103/PhysRevLett.85.491, URL https://link.aps.org/doi/10.1103/PhysRevLett.85.491.

[61] Wang L, Benenti G, Casati G, Li B. Ratchet effect and the transporting islands in the chaotic sea. Phys Rev Lett 2007;99:244101. http://dx.doi.org/10.1103/PhysRevLett.99.244101, URL https://link.aps.org/doi/10.1103/PhysRevLett.99.244101.

[62] Mugnaine M, Batista AM, Caldas IL, Szezech Jr JD, Viana RL. Ratchet current in nontwist Hamiltonian systems. Chaos 2020;30(9):093141. http://dx.doi.org/10.1063/5.0022073.

[63] Portela JSE, Caldas IL, Viana RL, Morrison PJ. Diffusive transport through a nontwist barrier in tokamaks. Int J Bifurcation Chaos 2007;17(05):1589–98. http://dx.doi.org/10.1142/S0218127407017926.

[64] Wurm A, Martini KM. Breakup of inverse golden mean shearless tori in the two-frequency standard nontwist map. Phys Lett A 2013;377(8):622–7. http://dx.doi.org/10.1016/j.physleta.2013.01.003, URL https://www.sciencedirect.com/science/article/pii/S0375960113000169.

[65] Balescu R. Aspects of anomalous transport in plasmas. Series in plasma physics, CRC Press; 2005, URL https://books.google.com.br/books?id=Yaupom_qdKIC.

[66] Horton W. Onset of stochasticity and the diffusion approximation in drift waves. Plasma Phys Control Fusion 1985;27(9):937. http://dx.doi.org/10.1088/0741-3335/27/9/001.

[67] Viana RL, Mugnaine M, Caldas IL. Hamiltonian description for magnetic field lines in fusion plasmas: A tutorial. Phys Plasmas 2023;30(9):090901. http://dx.doi.org/10.1063/5.0170345, arXiv:https://pubs.aip.org/aip/pop/article-pdf/doi/10.1063/5.0170345/19848429/090901_1_5.0170345.pdf.

[68] Horton W, Park H-B, Kwon J-M, Morrison DSPJ, Choi D-I. Drift wave test particle transport in reversed shear profile. Phys Plasmas 1998;5(11):3910–7. http://dx.doi.org/10.1063/1.873110.

[69] Souza LC, Mathias AC, Caldas IL, Elskens Y, Viana RL. Fractal and Wada escape basins in the chaotic particle drift motion in tokamaks with electrostatic fluctuations. Chaos 2023;33(8):083132. http://dx.doi.org/10.1063/5.0147679.

[70] Souza LC, Sales MR, Mugnaine M, Szezech JD, Caldas IL, Viana RL. Chaotic escape of impurities and sticky orbits in toroidal plasmas. Phys Rev E 2024;109:015202. http://dx.doi.org/10.1103/PhysRevE.109.015202, URL https://link.aps.org/doi/10.1103/PhysRevE.109.015202.

[71] Miyamoto K. Plasma physics for controlled fusion. Springer series on atomic, optical, and plasma physics, Springer-Verlag Berlin; 2016.

[72] Weiland J, Zagorodny A. Drift wave theory for transport in tokamaks. Rev Mod Plasma Phys 2019;3(1):8.

[73] Caldas I, Viana R, Szezech J, Portela J, Fonseca J, Roberto M, Martins C, da Silva E. Nontwist symplectic maps in tokamaks. Commun Nonlinear Sci Numer Simul 2012;17(5):2021–30. http://dx.doi.org/10.1016/j.cnsns.2011.05.040, special Issue: Mathematical Structure of Fluids and Plasmas. URL https://www.sciencedirect.com/science/article/pii/S1007570411002875.

[74] Chirikov BV. A universal instability of many-dimensional oscillator systems. Phys Rep 1979;52(5):263–379. http://dx.doi.org/10.1016/0370-1573(79)90023-1, URL https://www.sciencedirect.com/science/article/pii/0370157379900231.

[75] Lieberman MA, Lichtenberg AJ. Stochastic and adiabatic behavior of particles accelerated by periodic forces. Phys Rev A 1972;5:1852–66. http://dx.doi.org/10.1103/PhysRevA.5.1852, URL https://link.aps.org/doi/10.1103/PhysRevA.5.1852.

[76] da Silva JKL, Ladeira DG, Leonel ED, McClintock PVE, Kamphorst SO. Scaling properties of the Fermi-Ulam accelerator model. Braz J Phys 2006;36(3a):700–7. http://dx.doi.org/10.1590/S0103-97332006000500022, URL http://www.scielo.br/scielo.php?script=sci_arttext&pid=S0103-97332006000500022&lng=en&nrm=iso&tlng=en.

[77] Leonel ED, McClintock PVE. A hybrid Fermi–Ulam-bouncer model. J Phys A: Math Gen 2005;38(4):823. http://dx.doi.org/10.1088/0305-4470/38/4/004.

[78] Leonel ED, Livorati ALP. Describing Fermi acceleration with a scaling approach: The bouncer model revisited. Phys A 2008;387(5):1155–60. http://dx.doi.org/10.1016/j.physa.2007.10.037, URL https://www.sciencedirect.com/science/article/pii/S0378437107011259.

[79] Howard JE, Humpherys J. Nonmonotonic twist maps. Physica D 1995;80(3):256–76. http://dx.doi.org/10.1016/0167-2789(94)00180-X, URL https://www.sciencedirect.com/science/article/pii/016727899400180X.

[80] Leonel ED. Phase transition in dynamical systems: Defining classes of universality for two-dimensional Hamiltonian mappings via critical exponents. Math Probl Eng 2009;2009:367921. http://dx.doi.org/10.1155/2009/367921.

[81] de Oliveira JA, Bizão RA, Leonel ED. Finding critical exponents for two-dimensional Hamiltonian maps. Phys Rev E 2010;81:046212. http://dx.doi.org/10.1103/PhysRevE.81.046212, URL https://link.aps.org/doi/10.1103/PhysRevE.81.046212.

[82] de Oliveira JA, Dettmann CP, da Costa DR, Leonel ED. Scaling invariance of the diffusion coefficient in a family of two-dimensional Hamiltonian mappings. Phys Rev E 2013;87:062904. http://dx.doi.org/10.1103/PhysRevE.87.062904, URL https://link.aps.org/doi/10.1103/PhysRevE.87.062904.

[83] de Oliveira JA, da Costa DR, Leonel ED. Survival probability for chaotic particles in a set of area preserving maps. Eur Phys J Spec Top 2016;225(13):2751–61. http://dx.doi.org/10.1140/epjst/e2015-50330-y.

[84] Leonel ED, Yoshida M, de Oliveira JA. Characterization of a continuous phase transition in a chaotic system. Europhys Lett 2020;131(2):20002. http://dx.doi.org/10.1209/0295-5075/131/20002.

[85] Moser J. Monotone twist mappings and the calculus of variations. Ergodic Theory Dynam Systems 1986;6(3):401–13. http://dx.doi.org/10.1017/S0143385700003588.

[86] Virtanen P, Gommers R, Oliphant TE, Haberland M, Reddy T, Cournapeau D, Burovski E, Peterson P, Weckesser W, Bright J, van der Walt SJ, Brett M, Wilson J, Millman KJ, Mayorov N, Nelson ARJ, Jones E, Kern R, Larson E, Carey CJ, Polat İ, Feng Y, Moore EW, VanderPlas J, Laxalde D, Perktold J, Cimrman R, Henriksen I, Quintero EA, Harris CR, Archibald AM, Ribeiro AH, Pedregosa F, van Mulbregt P, SciPy 10 Contributors. SciPy 1.0: Fundamental algorithms for scientific computing in Python. Nature Methods 2020;17:261–72. http://dx.doi.org/10.1038/s41592-019-0686-2.

[87] Shimada I, Nagashima T. A numerical approach to ergodic problem of dissipative dynamical systems. Progr Theoret Phys 1979;61(6):1605–16. http://dx.doi.org/10.1143/PTP.61.1605.

[88] Benettin G, Galgani L, Giorgilli A, Strelcyn J-M. Lyapunov characteristic exponents for smooth dynamical systems and for Hamiltonian systems; a method for computing all of them. part 1: Theory. Meccanica 1980;15(1):9–20. http://dx.doi.org/10.1007/BF02128236.

[89] Wolf A, Swift JB, Swinney HL, Vastano JA. Determining Lyapunov exponents from a time series. Physica D 1985;16(3):285–317. http://dx.doi.org/10.1016/0167-2789(85)90011-9, URL https://www.sciencedirect.com/science/article/pii/0167278985900119.

[90] Eckmann JP, Ruelle D. Ergodic theory of chaos and strange attractors. Rev Modern Phys 1985;57:617–56. http://dx.doi.org/10.1103/RevModPhys.57.617, URL https://link.aps.org/doi/10.1103/RevModPhys.57.617.

[91] Leonel ED. Scaling Laws in Dynamical Systems. 1st ed.. Springer Singapore; 2021, http://dx.doi.org/10.1007/978-981-16-3544-1.

[92] Hansen M, Egydio de Carvalho R, Leonel ED. Influence of stability islands in the recurrence of particles in a static oval billiard with holes. Phys Lett A 2016;380(43):3634–9. http://dx.doi.org/10.1016/j.physleta.2016.09.009, URL https://www.sciencedirect.com/science/article/pii/S0375960116307654.

[93] Méndez-Bermúdez JA, Peralta-Martinez K, Sigarreta JM, Leonel ED. Leaking from the phase space of the Riemann-Liouville fractional standard map. Chaos Solitons Fractals 2023;172:113532. http://dx.doi.org/10.1016/j.chaos.2023.113532, URL https://www.sciencedirect.com/science/article/pii/S0960077923004332.

[94] Borin D. Caputo fractional standard map: Scaling invariance analyses. Chaos Solitons Fractals 2024;181:114597. http://dx.doi.org/10.1016/j.chaos.2024.114597, URL https://www.sciencedirect.com/science/article/pii/S0960077924001486.

[95] Leonel ED, McClintock PVE, da Silva JKL. Fermi-Ulam accelerator model under scaling analysis. Phys Rev Lett 2004;93:014101. http://dx.doi.org/10.1103/PhysRevLett.93.014101, URL https://link.aps.org/doi/10.1103/PhysRevLett.93.014101.

[96] Leonel ED, McClintock PVE. Chaotic properties of a time-modulated barrier. Phys Rev E 2004;70:016214. http://dx.doi.org/10.1103/PhysRevE.70.016214, URL https://link.aps.org/doi/10.1103/PhysRevE.70.016214.

[97] Leonel ED. Corrugated waveguide under scaling investigation. Phys Rev Lett 2007;98:114102. http://dx.doi.org/10.1103/PhysRevLett.98.114102, URL https://link.aps.org/doi/10.1103/PhysRevLett.98.114102.

[98] Livorati ALP, Ladeira DG, Leonel ED. Scaling investigation of Fermi acceleration on a dissipative bouncer model. Phys Rev E 2008;78:056205. http://dx.doi.org/10.1103/PhysRevE.78.056205, URL https://link.aps.org/doi/10.1103/PhysRevE.78.056205.

[99] Leonel ED, Penalva J, Teixeira RM, Costa Filho RN, Silva MR, de Oliveira JA. A dynamical phase transition for a family of Hamiltonian mappings: A phenomenological investigation to obtain the critical exponents. Phys Lett A 2015;379(32):1808–15. http://dx.doi.org/10.1016/j.physleta.2015.04.025, URL https://www.sciencedirect.com/science/article/pii/S0375960115003679.

[100] Miranda LKA, Kuwana CM, Huggler YH, da Fonseca AKP, Yoshida M, de Oliveira JA, Leonel ED. A short review of phase transition in a chaotic system. Eur Phys J Spec Top 2022;231(3):167–77. http://dx.doi.org/10.1140/epjs/s11734-021-00415-3.

[101] Spizzo G, White R, Maraschek M, Igochine V, Granucci G, Team TAU. Nonlocal transport in toroidal plasma devices. Nucl Fusion 2018;59(1):016019. http://dx.doi.org/10.1088/1741-4326/aaf07c.

[102] Barabási A-L, Stanley HE. Fractal concepts in surface growth. Cambridge University Press; 1995.

[103] Rolim Sales M. mrolims/nontwist-dynamical-system: v1.0.8. 2024, http://dx.doi.org/10.5281/zenodo.11154583.

[104] Rolim Sales M. mrolims/nontwist-dynamical-system. 2024, URL https://github.com/mrolims/nontwist-dynamical-system.git.